

See discussions, stats, and author profiles for this publication at: <https://www.researchgate.net/publication/352181219>

Design, modeling and control of a miniature bio-inspired amphibious spherical robot

Article in *Mechatronics* · May 2021

DOI: 10.1016/j.mechatronics.2021.102574

CITATIONS

0

READS

49

8 authors, including:



[Huiming Xing](#)

Harbin Engineering University

37 PUBLICATIONS 196 CITATIONS

[SEE PROFILE](#)



[Liwei Shi](#)

Kagawa University

90 PUBLICATIONS 1,401 CITATIONS

[SEE PROFILE](#)



[Hou Xihuan](#)

Beijing Institute of Technology

25 PUBLICATIONS 139 CITATIONS

[SEE PROFILE](#)



[Debin Xia](#)

Beijing Institute of Technology

18 PUBLICATIONS 45 CITATIONS

[SEE PROFILE](#)

Some of the authors of this publication are also working on these related projects:



Robotics and automation [View project](#)



Graduate Technological Innovation Project of Beijing Institute of Technology [View project](#)



Design, modeling and control of a miniature bio-inspired amphibious spherical robot

Huiming Xing^{a,b}, Liwei Shi^{a,*}, Xihuan Hou^a, Yu Liu^a, Yao Hu^a, Debin Xia^a, Zan Li^a, Shuxiang Guo^{a,c}

^a Key Laboratory of Convergence Medical Engineering System and Healthcare Technology, The Ministry of Industry and Information Technology, Beijing Institute of Technology, No.5, Zhongguancun South Street, Haidian District, Beijing 100081, China

^b College of Intelligent Systems Science and Engineering, Harbin Engineering University, Harbin, Heilongjiang Province, China

^c Faculty of Engineering, Kagawa University, Takamatsu, Kagawa, 760-8521, Japan

ARTICLE INFO

Keyword:

Bio-inspired robots
Real-time dynamic vectoring control
Amphibious spherical robot
Vectoring control

ABSTRACT

It is a huge challenge for an amphibious robot with a high locomotory performance to locomote in amphibious environments, including crawling on rough terrains, maneuvering underwater, and launching and landing motion between land and water. To deal with such a challenge, a miniature bio-inspired Amphibious Spherical Robot (ASRobot) with a Legged, Multi-vectorized Water-jet Composite Driving Mechanism (LMWCMDM) has been designed. In this paper, locomotory performance of the robot in amphibious field environments is studied. First, a simplified kinematic model was built to study crawling gaits, and with an online adjustment mechanism, the gaits were adjusted, enabling the robot to climb up slopes more stably. Then, using a dynamic underwater model, a real-time dynamic thrust vectoring allocation strategy is proposed to generate the water-jet thrust and joint angles using desired forces and torques computed by four parallel PID algorithms. Finally, a set of experiments were carried out to evaluate the performance of on land locomotion and underwater locomotion. Further, outdoor locomotion experiments including crawling on various terrains, launching and landing motion, were conducted in field environments. The results demonstrate that the robot prototype possesses the high locomotory performance which endows its wide application of disaster rescue, reconnaissance and resource exploration in amphibious environments.

1. Introduction

Recently, various autonomous amphibious robots have been developed as amphibious robot research gain importance. With land and underwater ability of amphibious robots, they are widely applied in a plenty of high-risk tasks, such as pollution detection, exploration and monitoring in amphibious zone, scientific investigation, search and rescue.

To realize multiple locomotion modes in amphibious environments, such as legged, wheeled, tracked, snake-like, undulating, oscillatory and propellered, a mass of research has been carried out to develop various novel driving mechanisms and robots. Different locomotion modes are proposed to different scenarios. Wheeled robots [1] deal with flat terrains, but cope poorly with uneven ground, while legged robots [2–4] crawl well on uneven terrains, but move slowly. Snake-inspired serpentine robots [5] do well on even terrains except that the

direction and velocity is hard to control. In aquatic environment, compared to the robots with oscillatory and undulatory abilities, screw propellers-driven robots have high stability and mobility. Therefore, many amphibious robots possess abilities of multiple locomotion modes.

AmphiHex-I [6], an amphibious robot, was developed using the transformable flipper legs which serves as “a drive wheel” for walking on land and an oscillatory leg in water. In littoral areas, the robot is able to traverse different terrains between land and water. To improve the performance on land and in water, a novel variable stiffness legs was proposed using a flexible flipper with the rigid fan-shaped leg structure [7]. The highest speed on land and in water improved 0.16 m/s and 0.18 bl/s, respectively, but it is not easy to keep the given pose and position in water. Based on an epicyclic gear mechanism (ePaddle-EGM), an amphibious robot [8–10] was proposed with an eccentric paddle mechanism. The robot is able to work with various on-land and underwater locomotion, such as rotational and oscillating paddling locomotion.

* Corresponding author.

E-mail address: shiliwei@bit.edu.cn (L. Shi).

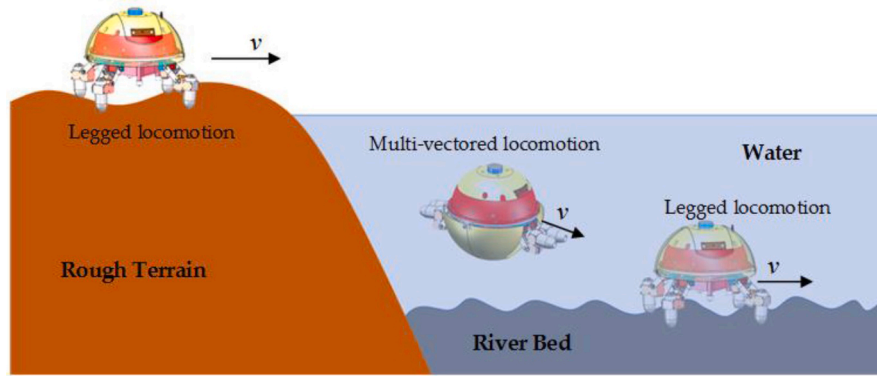


Fig. 1. Schematic diagram of the bio-inspired amphibious robot in amphibious zone.

In addition to these above amphibious robots, lots of bio-inspired amphibious robots have also been proposed widely, such as turtles, salamandra, Natatores [11] and snakes [12]. Inspired by snakes, a novel serpentine gait [13,14] was designed using the geometry mechanics. Inspired by salamander, a bio-amphibious robot (Salamandra robotica II) [15] was proposed with four legs and an active spine. The robot swims in water and walks on land with varieties of gaits using body-limb coordination and bodily undulation. In 2012, AmphiRobot-II [16–19], an amphibious fish-like robot, was proposed using a specialized swivel mechanism and a wheel-propeller-fin mechanism. This mechanism not only serves as a drive wheel for walking on ground, but also works as a screw propeller or pectoral fin for swimming underwater. In 2014, RoboTerp [20], a turtle-inspired quadrupedal amphibious robot, was proposed using a passive compliant mechanism attached to the lower leg. In 2012, MiniTurtle-I [21], an amphibious robot, was designed to transform on-land and underwater locomotion using a novel variable topology mechanism. Although these amphibious robots have realized the locomotion inspired by amphibious species, the efficiency of these mechanism is not high, and the flexible motion and pose and position maintenance with high precision is hard to be realized.

Inspired by turtles, a miniature bio-inspired amphibious spherical robot named ASRobot is proposed to monitor and explore amphibious and shallow river bed environments. As shown in Fig. 1, driven by a Legged, Multi-vectored Water-jet Composite Driving Mechanism (LMWCDDM), the robot crawls with legged locomotion on rough terrains and river bed. In water, a real-time dynamic thrust vectoring allocation strategy is proposed to realize hovering, vertical floating and sinking, rotational locomotion with zero-radius and 3-D waypoints tracking. The

main contributions of this paper are as follows: 1) The robot with spherical shape is able to rotate and tune orientations more easily than the streamlined design, which is quite essential for the robot in restricted narrow space. And the spherical body is a highly symmetrical structure, which is beneficial to the robot modeling. 2) An online gaits adjustment mechanism is proposed to climb up slopes more stably using a simplified kinematic model. 3) With the geometric principle of the force addition, a real-time dynamic thrust vectoring allocation strategy is proposed to transform the desired force and torque calculated by PID algorithms into the water-jet thrust and joint angles of each leg. “H” and “I” modes-based 3D waypoints tracking strategy is developed with four parallel PID sub-controllers.

The rest of the paper is organized as follows. Section II introduces ASRobot mechanism and LMWCDDM. On-land kinematic model, gaits design and gaits adjustment on a slope are presents in Section III. Section IV elaborates underwater dynamic model, force analysis and real-time dynamic thrust vectoring control strategy. Section V gives various experiments. This paper is concluded with future work in Section VI.

2. Modeling and kinematic analysis of the robot

2.1. The amphibious spherical robot

In consideration of the specific situation in uneven amphibious zone, a miniature bio-inspired amphibious robot was proposed using LMWCDDM. As shown in Fig. 3(a), the upper semi-spherical sealed cabin was separated into two parts to reduce the weight of the root. The first part (Top shell shown in Fig. 3) is used to hold the sensors, such as

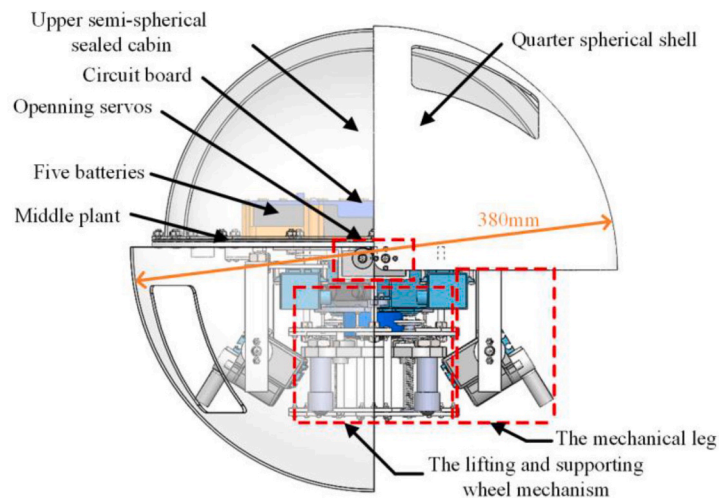


Fig. 2. Illustration of the previous bio-inspired amphibious spherical robot.

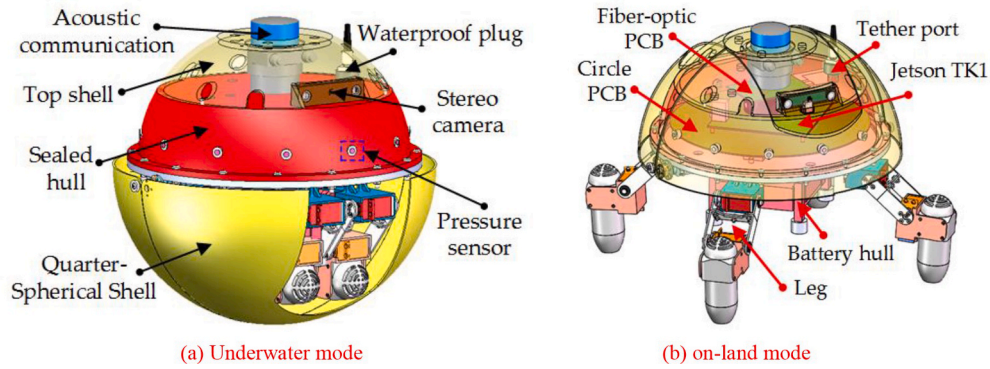


Fig. 3. Illustration of the novel bio-inspired amphibious spherical robot.

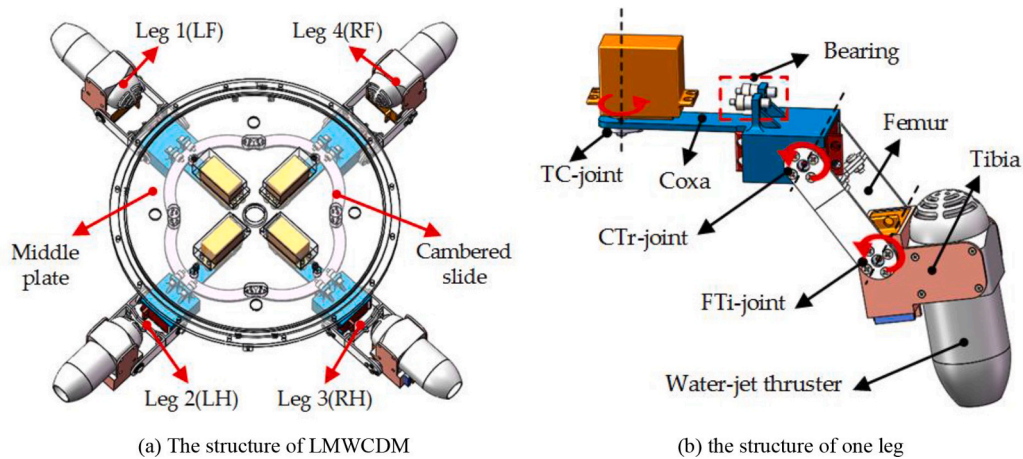


Fig. 4. Legged, Multi-Vectored Water-jet Composite Driving Mechanism.

communication module, stereo camera, and the second part (Sealed hull) can keep the fiber-optic Printed Circuit Board (PCB), motion control PCB, the main controller (Jetson TX2) and other sensors, such as Inertial Measurement Unit (IMU), pressure sensors. In order to improve the environment perception ability, a pressure sensors-based artificial lateral line is designed using 12 pressure sensors around the sealed hull. A tether port fixed on the second part is used to allow the robot to communicate via fiber-optic module and fiber cable. In order to keep the waterproofing performance for the sealed cabin, an O-ring is utilized between the sealed hull and the middle plant. Under the central plant is the composite driving mechanism and one detachable battery cabin with three batteries. Compared with the previous amphibious robot [22–25] shown in Fig. 2, the robot was improved as follows: 1) The upper semi-spherical sealed cabin used the up-down structure, instead of the

internal and external structure [23]. The water is able to enter the top shell from six holes, and the water will outflow when the robot climbs out of water, which can reduce the robot weight in air. 2) The mechanical leg was designed with 3 joints, replacing 2 joints of the previous robot. It extends the leg workspace and makes the robot leg more flexible. 3) The novel water-jet thruster [32] is developed to improve the motion ability. With the reasonable improvement, the dimension of the robot is reduced to be 300mm.

2.2. The legged, multi-vectored water-jet composite driving mechanism

For the proposed amphibious robot, terrestrial and aquatic locomotion rely on LMWCDM [27]. As shown in Fig. 4 (a), a radially free distributed structure around the robot is used to the composite driving mechanism. With the radial distribution of four legs, and the robot is more superior than the others [26] in rotation motion, especially in narrow restricted spaces. This driving mechanism contains four legs, and each leg includes three connecting rod parts that are regard as coxa, femur and tibia, respectively. Each leg has two bearings that assist the leg sliding freely between cambered slid and the middle plate. Each leg was actuated by three active joints. These joints connecting the three parts are named as follows: the joint connecting the body and coxa is define as Thoraco-Coxal joint (TC-joint), enabling the leg move forward or backward; the joint connecting the coxa and femur is termed as the Coxa-Trochanteral joint (CTr-joint), empowering leg’s elevation and depression; the joint connecting the femur and tibia is named as the Femur-Tibia joint (FTi-joint), which enables tibia’s extension and flexion. Therefore, each leg owns 3 degrees of freedom enabling the robot crawl more flexibly on ground than the previous robot [23]. As shown in Fig. 4(b), at the end of each leg is a water-jet thruster. In water,

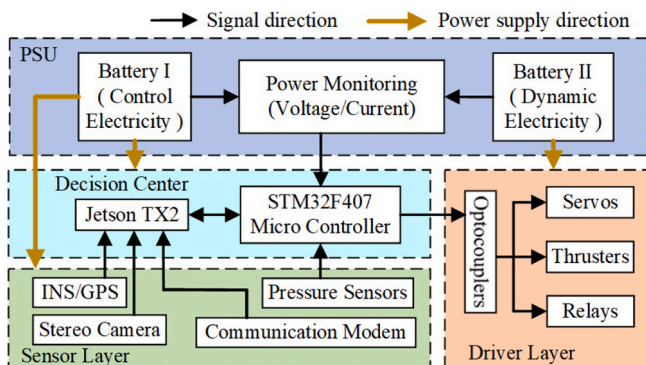


Fig. 5. The block diagram of control system.

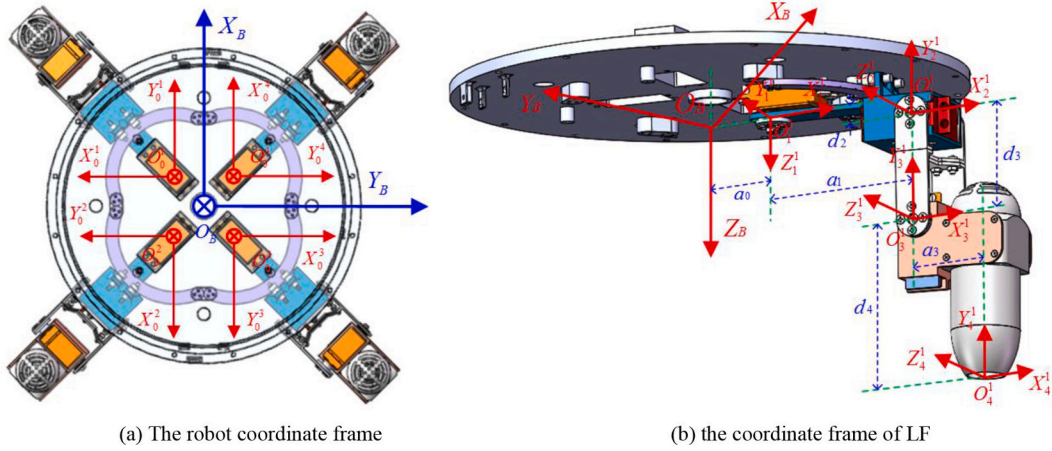


Fig. 6. Denavit-Hartenberg (DH) Model.

considering the water-jet thruster direction varying with legs control, a real-time dynamic thrust vectoring allocation strategy was proposed to generate the desired forces and torques. Jin *et al.* proposed a tilt thrusting underwater robot (TTURT) [28] with four tilting thrusters. Four tilting propellers have a tangentially free distribution in the edge of body frame diagonally. These robots [29, 30] with this kind of distribution have a good performance of posture control, but it will consume more energy in the long distance convey. This proposed mechanism with a radially free distribution is able to overcome these problems. With various leg configurations, the robot is able to realize high precision of position and orientation control simultaneously.

2.3. The control system

To improve the stability and logic of the circuit (Fig. 5), it is divided into four parts: Power Supply Unit (PSU), Decision-Making Center (DMC), sensor layer and driver layer. A powerful, stabilized, isolated PSU is quite essential to a robot. Before the robot crawls, the robot needs to stand up. As the robot starts to stand up, twelve servos require electricity simultaneously, which triggers a sudden surge current that challenges the processors and sensors. Therefore, the control and dynamic electricity is essential to separated. And we used three 7.4-V batteries, one (Battery II) of which powers DMC and sensor layer, and two (Battery I) of which provide power to driver layer. In order to isolate the control and dynamic electricity, they are required to not be common-grounded; DMC outputs PWM and GPIO signals to the motors and relays in dynamic electricity using optocouplers which transform photoelectric signals. The embedded computer (Jetson TX2) and auxiliary controller (stm32F407 micro controller) are applied to the robot, which possesses the computational capabilities for the intelligence and function. To explore and perceive in amphibious environments, the robot carries an Inertial Navigation System (INS), a Global Positioning System (GPS), stereo cameras, 12 pressure sensors around the sealed hull, and a communication modem. As shown in Fig. 5, only information of pressure sensors was collected by auxiliary controller using IIC. Considering real-time communication between embedded computer and the micro controller, Universal Asynchronous Receiver Transmitter (UART) is utilized.

3. Legged locomotion

3.1. Forward and inverse kinematic model on land

The robot crawls on land and on the river bed with legged locomotion. To present the legged locomotion simply, four legs were named as LF (Left Foreleg), LH (Left Hind leg), RH (Right Hind leg), and RF (Right

Table I
Denavit-Hartenberg (DH) parameters of lf.

Joint j	θ_j^i	α_{j-1}^i	a_{j-1}^i	d_j^i	θ_j^i
1	$\theta_1^1(0)$	0	a_0	$d_2(10)$	$(0, \pi/2)$
2	$\theta_2^1(0)$	$-\pi/2$	$a_1(97)$	0	$(-\pi/4, \pi/3)$
3	$\theta_3^1(0)$	0	a_2	$d_3(60)$	$(-\pi/6, \pi/2)$
4	0	0	$a_3(33)$	$d_4(85)$	0

Foreleg). The body-fixed coordinate frame is shown in Fig. 6 (a), and it located at the geometrical center of the body which is the same horizontal plane with the TC-joints of four legs. X_B , Y_B and Z_B axes point to the forward direction, the rightward direction and the downward direction (perpendicular to the body's horizontal plane). The coordinate frame $\{O_0^i\}$ indicates the base coordinate of the leg, and i is the leg number ($i = 1$ for LF, $i = 2$ for LH, $i = 3$ for RH, and $i = 4$ for RF). The coordinate frames $\{O_1^i\}$, $\{O_2^i\}$, $\{O_3^i\}$ and $\{O_4^i\}$ are built in TC-joint, CT-joint, FTi-joint and the toe, respectively. Fig. 6(b) shows the coordinate frames of LF.

Denavit-Hartenberg (D-H) parameters of LF is shown in Table 1. θ_j^i and d_j^i indicate the joint angle and the distance between the joint $j-1$ and j of leg i , respectively. α_{j-1}^i and a_{j-1}^i represent the torsional angle and the length of the bar $j-1$ of leg i , respectively. r is the horizontal distance from the center of the robot to the TC-joint [31].

Using the D-H homogeneous transformation formula in the driven-axis context, the toe position of the LF in terms of the coordinate frame $\{O_0^1\}$ can be obtained as follows:

$$\mathbf{p}^1 = \begin{bmatrix} p_x^1 \\ p_y^1 \\ p_z^1 \end{bmatrix} = \begin{bmatrix} c_1^1 c_{23}^1 a_3 + c_1^1 s_{23}^1 d_4 + c_1^1 s_2^1 d_3 + c_1^1 a_1 \\ s_1^1 c_{23}^1 a_3 + s_1^1 s_{23}^1 d_4 + s_1^1 s_2^1 d_3 + s_1^1 a_1 \\ -s_{23}^1 a_3 + c_{23}^1 d_4 + c_2^1 d_3 + d_2 \end{bmatrix} \quad (1)$$

where, $a = \sqrt{2}/2, s_j^i = \sin \theta_j^i, c_j^i = \cos \theta_j^i, s_{jk}^i = \sin(\theta_j^i + \theta_k^i)$ and $c_{jk}^i = \cos(\theta_j^i + \theta_k^i)$, $(cs)_j^i = c_j^i - s_j^i$ ($i = 1, 2, 3, 4$ and $j, k = 1, 2, 3$).

Similarly, equations of LH, RH and RF also can be obtained by the same procedure of LF. The forward kinematic model can be succinctly written as Eq. (2).

$${}^B \mathbf{p}_{loc}^B = FK(\theta) \quad (2)$$

where, FK represents the forward kinematics, allowing mapping from the joint space to the Cartesian space.

The movement can be calculated using the inverse kinematic model.

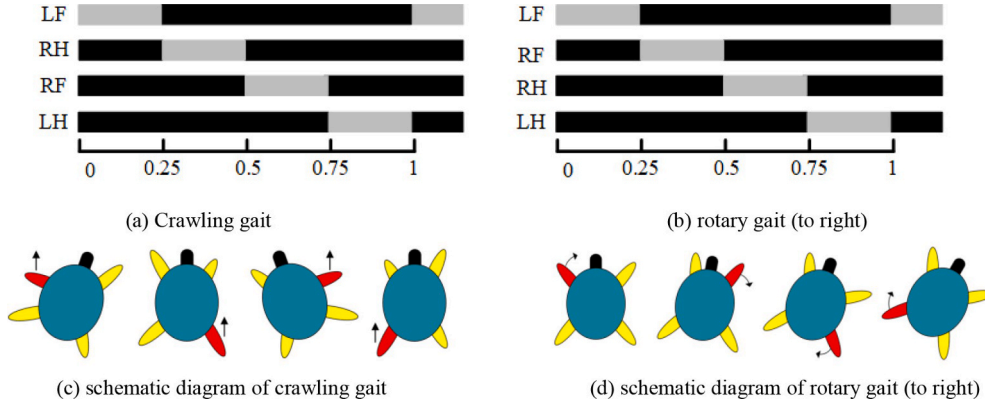


Fig. 7. The sequence of the gaits.

Employing the forward kinematic model, the inverse kinematic equations can be obtained by Eq. (3).

$$\begin{cases} \theta_1^1 = \text{atan2}(p_y^1, p_x^1) \\ \theta_2^1 = \text{atan2}(m, n) - \text{atan2}(k, \pm\sqrt{m^2 + n^2 - k^2}) \\ \theta_3^1 = \text{atan2}(-a_3, d_4) - \text{atan2}(t, \pm\sqrt{a_3^2 + d_4^2 - t^2}) \end{cases} \quad (3)$$

where, $m = c_1^1 p_x^1 + s_1^1 p_y^1 - a_1$, $t = (m^2 + n^2 - a_3^2 - d_4^2 - d_3^2) / 2d_3$, $n = p_z^1 - d_2$ and $-s_3^1 a_3 + c_3^1 d_4 + d_3 = k$.

Similarly, equations of LH, RH and RF also can be obtained by the same procedure. The inverse kinematic model can be succinctly written as Eq. (4).

$$\theta = IK({}^B P_{\text{toe}}) \quad (4)$$

where IK refers to the inverse kinematics, allowing mapping from the Cartesian space to the joint space.

3.2. Gaits design

Gaits, such as walking gaits, trotting gaits and tripod gaits, have been developed. Considering applications in the amphibious zone, ASRobot is required to walk flexibly on rough terrains and on the river bed and swim swiftly in water. Compared with quadruped robots with the same size, the proposed robot needs a heavy body to keep the gravity larger than the buoyancy in water. The miniaturization and waterproofing design of the mechanical leg limits its driving performance. Although the robot is designed with compact structure, the weight is up to 6.7Kg. The robot uses three and less legs to support the body, which is a

challenge for the mechanical legs. Therefore, a crawling gait and a rotary gait were developed to ASRobot, which allows ASRobot crawl like a turtle. Fig. 7 (a) shows the sequence of the crawling gait in one cycle. The gray and black bars indicate the transfer phase and the support phase, respectively. In the transfer phase, the robot lifts the leg and falls to the ground. The support phase is the time that the leg is on the ground in one cycle. Fig. 7 (c) shows schematic diagram of the crawling gait sequence “LF→RH→RF→LH”, and the red and yellow legs indicate the leg in the transfer phase and support phase, respectively. Fig. 7 (b) describes the sequence of the rotary gait. Compared to the crawling gait, the main difference is the swing direction and sequence of the leg. The robot rotates to right when all legs swing to right in transfer phase, and vice versa. Fig. 7 (d) shows that the robot rotates to right with gait sequence “LF→RF→RH→LH”. For two gaits, the robot is always moving the body during each cycle. Compared with the previous robot with two joints in one leg, ASRobot with three joints in one leg benefits in adaptability, flexibility and maneuverability.

3.3. Gaits adjustment on a slope

For the amphibious robot, here are some situations that the robot needs to crawl into the water from the riverbank and walk on a slope. In the flat ground, the positions of the toes always keep in the same horizon. Fig. 8 (a) describes the climbing motion using the designed gaits. When climbing on a slope, the body of the robot inclines. The center of gravity moves backward and upward, and the friction force decreases. These aspects will make the robot slip down or roll down from the slope. Therefore, the gait on the slope needs to be adjusted. To keep the robot horizontal and lower the center of gravity, the toe positions of legs are arranged according to the angle of the slope. Using Eq. (3), the adjusted angles will be calculated and added to the three joints of each leg. As

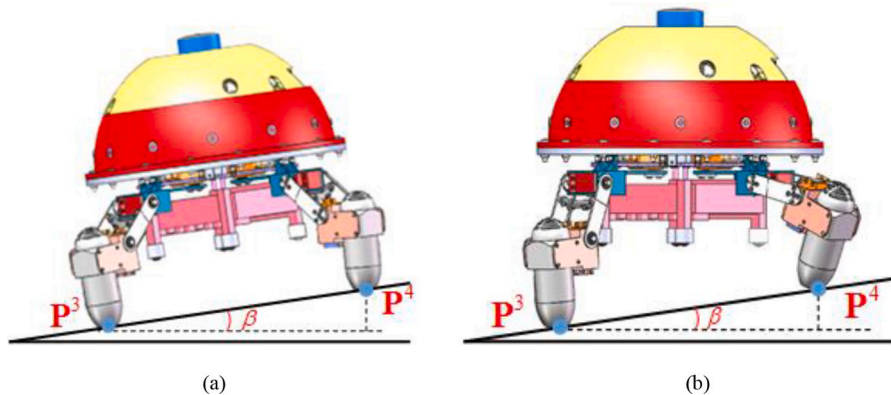


Fig. 8. The diagram of crawling gait on the slope.

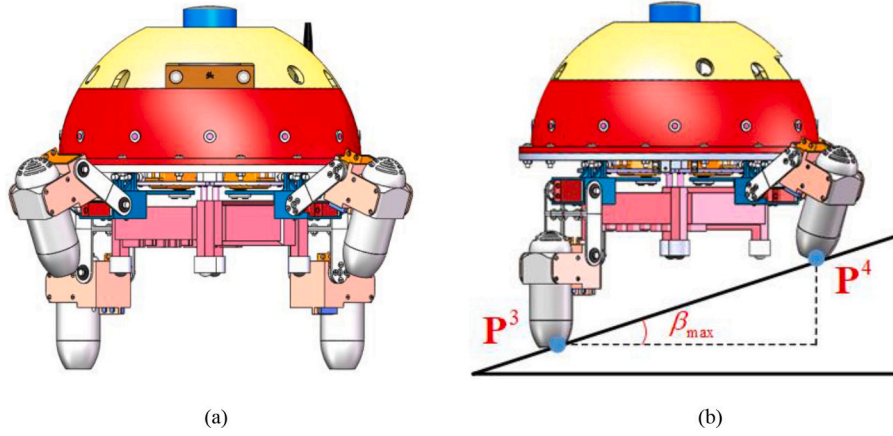


Fig. 9. The critical situation of crawling gait on the slope.

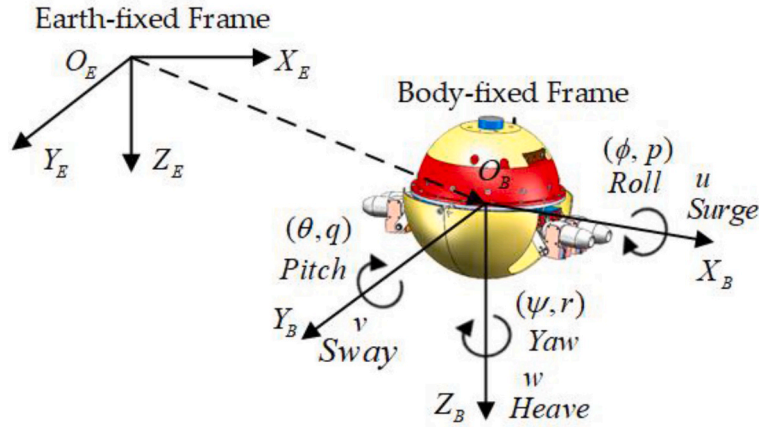


Fig. 10. Kinematic Frame of ASRobot.

shown in Fig. 8 (b), the right foreleg and the right hind leg are in the initial position, the coordinates of the landing points P^3 and P^4 are represented as

$$p_z^4 - p_z^3 = (p_y^4 - p_y^3) \tan \beta \quad (5)$$

where p_z^3 and p_z^4 are the position in Z axis of RH and RF, β represents the slope angle which is measured via the MEMS IMU, and the pose of the robot is estimated with Extended Kalman Filter (EKF).

Limited by the mechanical legs structure, the robot only climbs gentle slopes. Fig. 9 shows the case of RH and RF on a critical slope. In this case, LH and RH are vertical to the horizontal plane. For LF and RF, the robot tries its best to lift the two legs, and the limit angle climbing on the slope are calculated using Eqs. (1) and (2). Consequently, due to the limitation of the mechanical structure, the robot was capable of climbing slopes no larger than $\beta_{max} = 18\text{deg}$ in theory. The performance of climbing slope mainly is restricted by the vertical distance between two front legs and two hind legs. The longer legs will generate larger vertical distance. Therefore, a longer leg design is a good solution to make the robot climb the slopes larger than 18 deg. And we will be focused on it in the future.

4. Underwater locomotion control

Jin et al. proposed a switching control strategy to realize the hovering control of TTURT. The propellers cannot be tilted continuously between the vertical mode and the horizontal mode. Owing to the switching time between different modes, it will increase the error. Therefore, a real-

time dynamic thrust vectoring control with a continuous tilting angle of joints for ASRobot is proposed.

4.1. Dynamics model

To describe the complex motion of ASRobot in 4 degree of freedom (DOF) simply, a Newton-Euler formalism is utilized. To describe the robot motion simply, two reference coordinate frames were depicted in Fig. 10, one named earth-fixed frame $\{O_E-X_EY_EZ_E\}$, located on the earth, and the other one is body-fixed coordinate frame $\{O_B-X_BY_BZ_B\}$, placed at the center of robot gravity. The spatial position and orientation of ASRobot can be expressed by the state vector $\eta = [x, y, z, \phi, \theta, \psi]^T$, where $x, y, z, \phi, \theta, \psi$ present surge, sway, heave, roll, pitch and yaw in Earth-fixed frame, respectively. Let $\mathbf{v} = [u, v, w, p, q, r]^T$ be corresponding linear and angular velocity state vector, and $[u, v, w]$ and $[p, q, r]$ are defined as linear velocities and angular velocities at body-fixed frame, respectively. The relations between position state vector η and the velocity state vector \mathbf{v} is given as follows:

$$\dot{\eta} = J(\eta)\mathbf{v} \quad (6)$$

where, $J \in \mathbb{R}^{6 \times 6}$ represents the rotation matrix from body-fixed coordinate frame to earth-fixed coordinate frame.

The dynamics model is described as:

$$\mathbf{M}\dot{\mathbf{v}} + \mathbf{C}(\mathbf{v})\mathbf{v} + \mathbf{D}(\mathbf{v})\mathbf{v} + \mathbf{g}(\eta) = \mathbf{B}\boldsymbol{\tau} \quad (7)$$

where \mathbf{M} represents the mass and inertia matrix, \mathbf{C} is the Coriolis centripetal matrix, \mathbf{D} is the linear damping matrix, $\mathbf{g}(\eta)$ is the gravity and the

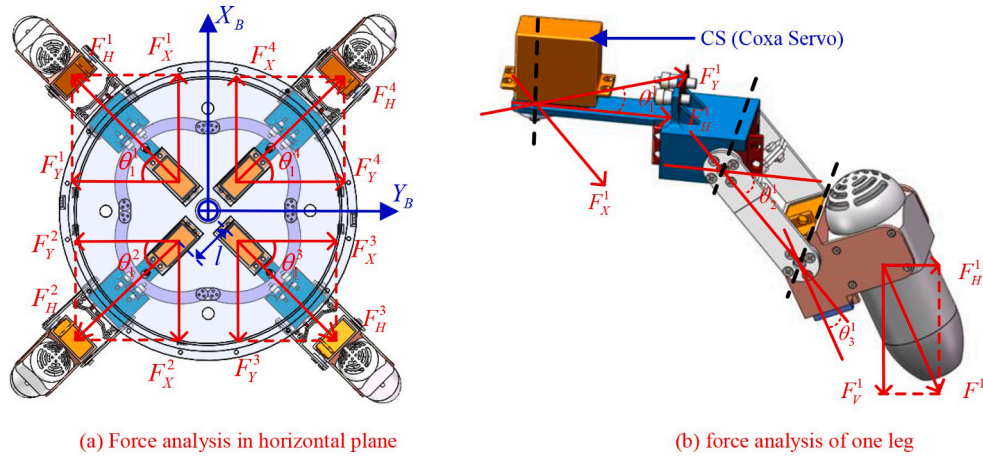


Fig. 11. The force analysis of the propulsion system.

buoyancy vector, and τ is the thrust vector generated by multi-vectorred water-jet propulsion system of the robot. Taking the geometrical properties of the high symmetrical structure into consideration, we made four hypotheses to simplify the dynamic model: (1) The moving velocity is lower than 0.6m/s, which satisfies hydrodynamic damping low speed motion condition. (2) The underwater motion is decoupled into horizontal model and vertical model. (3) Owing to the high symmetry of the robot, the surge motion and sway motion have the same hydrodynamic characteristics. (4) During underwater motion, the pitch and roll are small and can be ignored.

4.2. Force and moment analysis

As shown in Fig. 11, CS (Coxa Servo) is placed with a distance l from the center of ASRobot, and each leg is rotated by CS in the horizontal plane. Avoiding legs bump, each CS rotates within the angle bound $\theta_1 \in [-\pi/4, \pi/4]$ (rad).

The thrust along the X axis is:

$$F_X = -F^1 s_1^1 c_{23}^1 + F^2 s_1^2 c_{23}^2 + F^3 s_1^3 c_{23}^3 - F^4 s_1^4 c_{23}^4 \quad (8)$$

The thrust along the Y axis is:

$$F_Y = -F^1 c_1^1 c_{23}^1 + F^2 c_1^2 c_{23}^2 + F^3 c_1^3 c_{23}^3 - F^4 c_1^4 c_{23}^4 \quad (9)$$

The moment around the Z axis is:

$$T_Z = al[F^1 (cs)_1^1 c_{23}^1 + F^2 (cs)_1^2 c_{23}^2 + F^3 (cs)_1^3 c_{23}^3 + F^4 (cs)_1^4 c_{23}^4] \quad (10)$$

The vertical force along the Z axis of ASRobot is shown in Fig. 11. The

total vertical force on the Z axis:

$$F_Z = F^1 s_{23}^1 + F^2 s_{23}^2 + F^3 s_{23}^3 + F^4 s_{23}^4 \quad (11)$$

The moment around the X axis is:

$$T_X = al(-F^1 s_{23}^1 - F^2 s_{23}^2 + F^3 s_{23}^3 + F^4 s_{23}^4) \quad (12)$$

The moment around the Y axis is:

$$T_Y = al(-F^1 s_{23}^1 + F^2 s_{23}^2 + F^3 s_{23}^3 - F^4 s_{23}^4) \quad (13)$$

Hence, the force matrix $\mathbf{F}_B = [F_X \ F_Y \ F_Z]^T$ can be obtained as follows:

$$\mathbf{F}_B = \mathbf{M}_F \mathbf{F}_P \quad (14)$$

where, the force vector of four propellers $\mathbf{F}_P = [F^1 \ F^2 \ F^3 \ F^4]^T$, and

$$\mathbf{M}_F = \begin{bmatrix} -s_1^1 c_{23}^1 & s_1^2 c_{23}^2 & s_1^3 c_{23}^3 & -s_1^4 c_{23}^4 \\ c_1^1 c_{23}^1 & c_1^2 c_{23}^2 & -c_1^3 c_{23}^3 & -c_1^4 c_{23}^4 \\ s_{23}^1 & s_{23}^2 & s_{23}^3 & s_{23}^4 \end{bmatrix} \quad (15)$$

And, the moment matrix $\mathbf{T}_B = [T_X \ T_Y \ T_Z]^T$ can be obtained by Eq. (16).

$$\mathbf{T}_B = al\mathbf{M}_T \mathbf{F}_P \quad (16)$$

Therefore, the force and moment vector can be obtained by

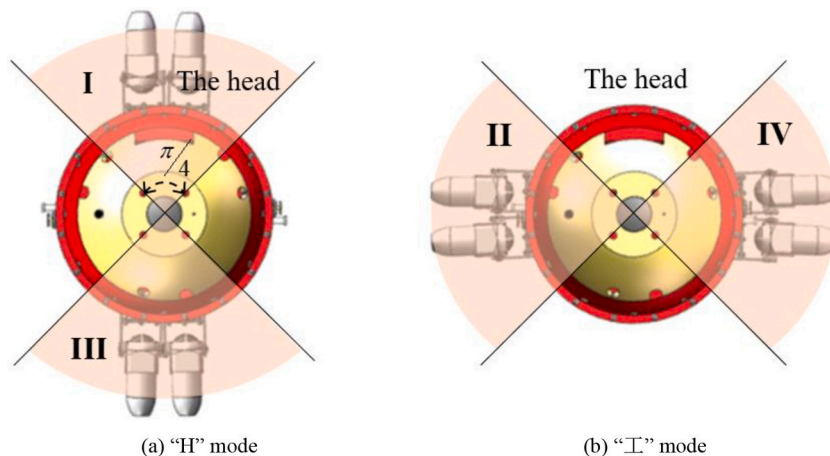


Fig. 12. Underwater locomotion modes.

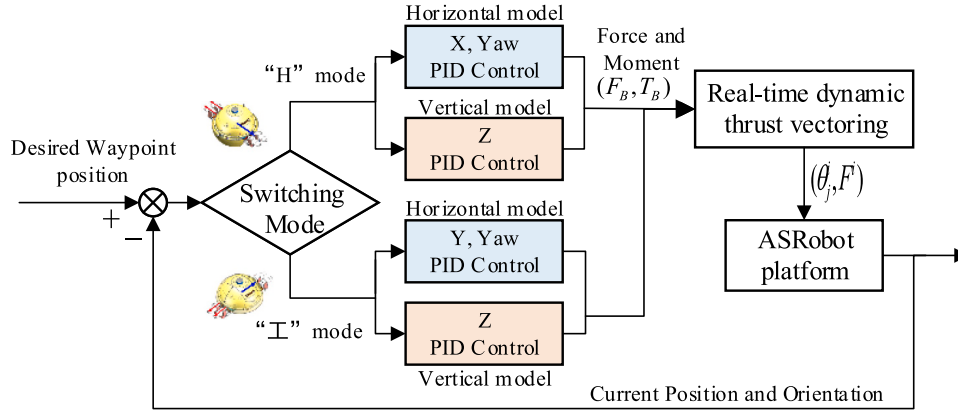


Fig. 13. Block diagram of real-time dynamic thrust vectoring control.

$$B\tau = \begin{bmatrix} s_1^1 c_{23}^1 & -s_1^2 c_{23}^2 & -s_1^3 c_{23}^3 & s_1^4 c_{23}^4 \\ -c_1^1 c_{23}^1 & -c_1^2 c_{23}^2 & c_1^3 c_{23}^3 & c_1^4 c_{23}^4 \\ s_{23}^1 & s_{23}^2 & s_{23}^3 & s_{23}^4 \\ -als_{23}^1 & -als_{23}^2 & als_{23}^3 & als_{23}^4 \\ -als_{23}^1 & als_{23}^2 & als_{23}^3 & -als_{23}^4 \\ al(cs)_1^1 c_{23}^1 & -al(cs)_1^2 c_{23}^2 & al(cs)_1^3 c_{23}^3 & -al(cs)_1^4 c_{23}^4 \end{bmatrix} \begin{bmatrix} F^1 \\ F^2 \\ F^3 \\ F^4 \end{bmatrix} \quad (17)$$

4.3. Real-time dynamic thrust vectoring control

Avoiding the error caused by the switching time between different modes [27], a real-time dynamic thrust vectoring control was proposed for ASRobot in “H” and “I” modes. As shown in Fig. 12, with adjusting the water-jet force and the rotational angle of CTR-joint and FTi-joint in real time, the robot is able to move laterally and longitudinally, sink, float and turn simultaneously in “H” and “I” modes. But the difference of two modes is “H” mode for forward and backward movement and “I” mode for leftward and rightward movement. In underwater waypoints tracking motion, four quadrants I, II, III, and IV shown in Fig. 12 were separated according to the robot. If the waypoint is in I and III, “H” mode is adopted. However, if the waypoint is in II or IV, the robot will rotate more than 45 deg in “H” mode, which increases the movement time. Therefore, “I” locomotion mode is proposed to deal with this case effectively. The condition of switching mode shown in Fig. 13 is able to be determined that “H” mode is for I and III areas and “I” mode for II and IV areas.

For the strongly coupled system of ASRobot, the control model is decoupled into two subsystems, i.e., horizontal model and vertical model. As shown in Fig. 13, forward and backward movement and yaw control (i.e., turning movement) were included in horizontal model, and depth control were considered in vertical model. The robot position and the waypoint i position are defined as $p_r(x_r, y_r, z_r)$ and $p_w^i(x_w^i, y_w^i, z_w^i)$, respectively. The angle from the robot position to the waypoint i position is $\gamma = \arctan[(y_w^i - y_r)/(x_w^i - x_r)]$. The position (x_r, y_r) , depth value z_r and yaw angle ψ are obtained by vision localization system, IMU and the pressure sensor, respectively. Then, the errors vector $\mathbf{e}(k)$ at time k is obtained as follows: $\mathbf{e}(k) = [x_w - x_r \quad y_w - y_r \quad z_w - z_r \quad 0 \quad 0 \quad \gamma - \psi]^T$. By means of position and orientation as feedback, forces \mathbf{F}_B and moments \mathbf{T}_B were obtained by Eq. (18) using four parallel PID algorithms.

$$\begin{bmatrix} \mathbf{F}_B \\ \mathbf{T}_B \end{bmatrix} = \mathbf{k}_p \mathbf{e}(k) + \mathbf{k}_i \sum_{k=0}^k \mathbf{e}(k) + \mathbf{k}_d [\mathbf{e}(k) - \mathbf{e}(k-1)] \quad (18)$$

where, $\mathbf{k}_{p,i,d} = \text{diag}(k_{p,i,d}^x \quad k_{p,i,d}^y \quad k_{p,i,d}^z \quad 0 \quad 0 \quad k_{p,i,d}^\psi)$ is the parameters of PID algorithm. And the water-jet thrust F^i and angle θ_j^i of each leg were calculated using a real-time dynamic thrust vectoring allocation

strategy. Then, the robot is able to swim in the aquatic environment and track 3-D waypoints with multiple movements simultaneously, such as forward or backward movement, turning and sinking or floating in “H” mode, leftward or rightward movement, turning and sinking or floating in “I” mode.

Eq. (19) was obtained in horizontal and vertical model.

$$\begin{cases} F_x^1 - F_x^2 - F_x^3 + F_x^4 = F_x \\ alF_x^1 - alF_x^2 + alF_x^3 - alF_x^4 = T_z \end{cases} \quad (19)$$

Assumption: In order to maintain the balance of the water-jet forces, equation $F_x^1 - F_x^3 = F_x^4 - F_x^2$ was considered.

Then, the water-jet force of each thruster was obtained as follows:

$$\begin{cases} F_x^1 = T_z/2al + F_x^4 \\ F_x^2 = -F_x^4/2 + F_x^4 \\ F_x^3 = (T_z - F_x)/2al + F_x^4 \\ F_x^4 = F_x^4 \end{cases} \quad (20)$$

To minimize the thrust, assume that F_x^4 is zero firstly. Then, a special solution was obtained. The minimal thrust was calculated by $F_{\min} = \min\{F_x^i\}$. Then the thrust was obtained.

$$f_x^i = F_x^i - \min\{F_x^i\} \quad (21)$$

In vertical model, the control model was described as:

$$\begin{cases} F_z^1 + F_z^2 + F_z^3 + F_z^4 = F_z \\ -alF_z^1 + alF_z^2 + alF_z^3 - alF_z^4 = T_y \\ -alF_z^1 - alF_z^2 + alF_z^3 + alF_z^4 = T_x \end{cases} \quad (22)$$

Then, the thrust was computed as

$$\begin{cases} F_z^1 = (alF_z - T_y)/2al - F_z^4 \\ F_z^2 = (alF_y - T_x)/2al + F_z^4 \\ F_z^3 = (alF_z + T_x)/2al - F_z^4 \\ F_x^4 = F_x^4 \end{cases} \quad (23)$$

F_z^1 and F_z^3 decreases as F_z^4 increases, but F_z^2 and F_z^4 increase as F_z^4 increases. In order to minimize the maximal thrust, F_x^4 was set as zero. Then it was defined as:

$$F_x^4 = (\max\{F_z^1, F_z^3\} - \max\{F_z^2, F_z^4\})/2 \quad (24)$$

Then, the forces $(f_z^1, f_z^2$ and $f_z^3)$ were determined by

Algorithm 1

The optimization algorithm of angle and thrust.

-
- 1: **Step1: angle optimization**
 - 2: IF $\min\{\theta_3\} < (\theta_3)_{\min}$
 - 3: Get index i of minimal angle θ_3 and set $m = i$
 - 4: $d = \frac{f_Z^m}{\tan((\theta_3)_{\min})} - f_X^m$
 - 5: Calculate the thrust $f_X^i = f_X^m + d$ and $F^i = \sqrt{(f_X^i)^2 + (f_Z^i)^2}$
 - 6: Calculate the angle $\theta_3^i = \arctan(f_Z^i / f_X^i)$
 - 7: **Step2: thrust optimization**
 - 8: IF $\max\{F^i\} > F_{\max}$
 - 9: Get index i of maximal thrust and set $n = i$
 - 10: $ratio = F_{\max} / F^n$
 - 11: Calculate the thrust $F^i = F^n \times ratio$
-

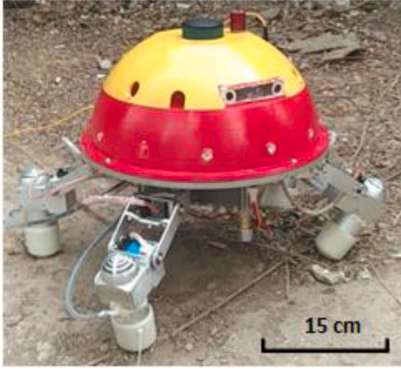


Fig. 14. The ASRobot prototype.

$$\begin{cases} f_Z^1 = F_Z^1 - F_Z^4 \\ f_Z^2 = F_Z^2 + F_Z^4 \\ f_Z^3 = F_Z^2 - F_Z^4 \\ f_Z^4 = F_Z^4 \end{cases} \quad (25)$$

With the obtained force f_X^i and f_Z^i , the water-jet thrusts were calculated by Eq. (26).

$$F^i = \sqrt{(f_X^i)^2 + (f_Z^i)^2} \quad (26)$$

And the angle is able to be synthesized according to Eq. (17). Owing to the valid wide range of angle θ_3 , angle θ_2 was set to be a specific value, which keeps the Femur horizontal. Therefore, the angle θ_3 was obtained

by

$$\theta_3^i = \arctan(f_Z^i / f_X^i) \quad (27)$$

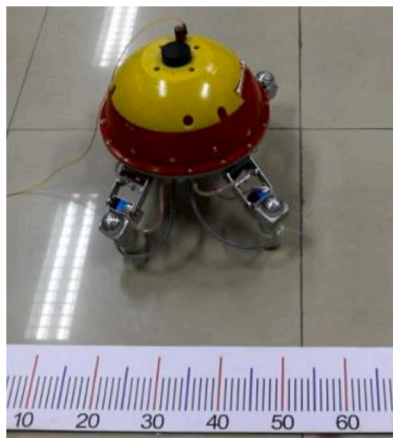
However, due to the limitations of the water-jet thrust ($0 \leq F^i \leq 2.4N, F_{\max} = 2.4N$) and the angle ($-\pi/6 \leq \theta_3^i \leq \pi/2, (\theta_3)_{\min} = -\pi/6$), the calculated angle cannot be reached. Therefore, an optimization algorithm was proposed to confirm these limitations as Algorithm 1.

5. Experiments and results**5.1. The robot prototype**

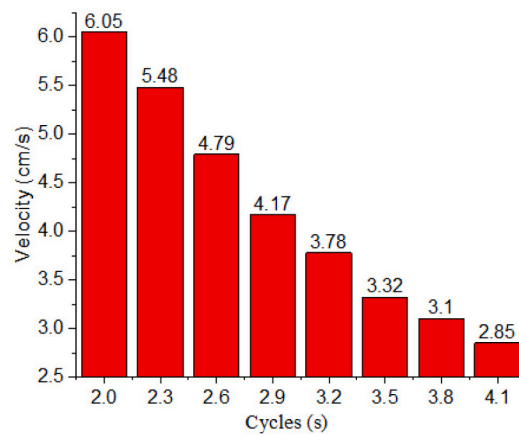
A robot prototype [31] with LMWCMD was constructed. This robot, depicted in Fig. 14, uses four submersible water-jet thrusters [32] with the long duct design. On land, the thruster is regarded as one part of the leg. In water, the water-jet direction was adjusted via three servo motors in one leg. Allowing for the energy density of the leg walking on land and the switching speed of water-jet direction, GWD SHARK servomotor with 36Kg·cm and 0.1s/60deg is utilized to the proposed robot. With a reasonable arrangement of sensors and LMWCMD in the compact robot, the dimension of the proposed spherical robot is set to be 300mm. The mass of the robot prototype in air is 6.7Kg. One detachable battery cabin includes three batteries. One (7.4V, 4400mAh) powers the decision center which contains an embedded computer Jetson TX2, and an auxiliary controller (stm32F407), and sensors and fiber-optic board, and two (7.4V, 1320mAh) power the driver layer containing 14 servo motors and four thrusters. Battery working time is typically 90 min during experiments. In view of yaw stabilization and orientation control, a six-axis 3DM-GX5-45 IMU is utilized. For measuring depth, 12 MS5837-02BA pressure sensors are embedded around the sealed hull. Photograph of the robot prototype is shown in Fig. 14. The high symmetry of the robot benefits the robot dynamics modeling and control.

5.2. Crawling experiments on land and in aquatic environment**(1) Experiments on the Flat Ground**

For the turtle-inspired robot, crawling on flat ground is essential. The crawling gait designed in Section III was realized for ASRobot. Allowing for the constraints of the leg structure, such as the angle limitation of joints rotation and the length of links, the longest stride length is 15cm. Using this stride length, the robot is able to walk steadily. Considering the limited rotation performance of servo motors, the cycle time of the crawling gait was set as 2.0s, 2.3s, 2.6s, 2.9s, 3.2s, 3.5s, 3.5s, 3.8s, 4.1s.



(a) Experimental setup



(b) the velocity of crawling

Fig. 15. ASRobot crawling experiment.

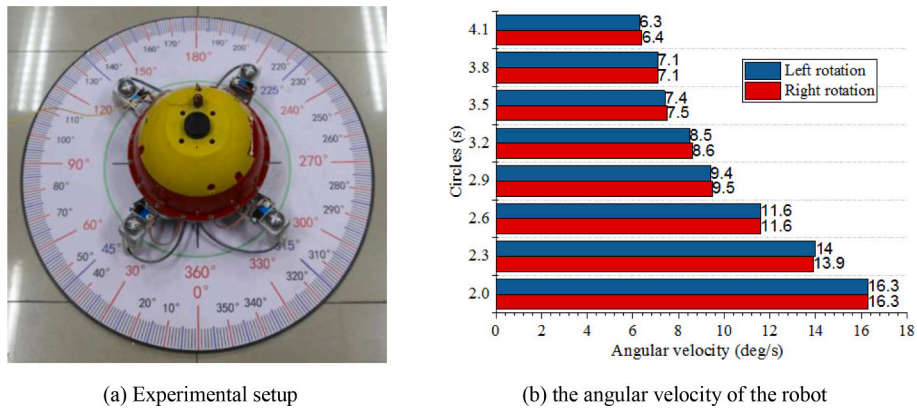


Fig. 16. ASRobot rotating on smooth flat board.

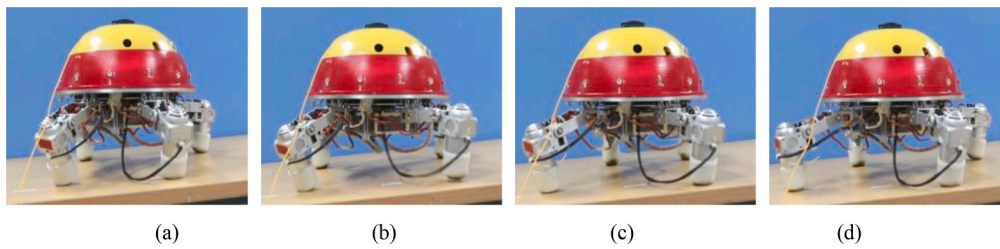


Fig. 17. Snapshots of ASRobot climbing on a slope.

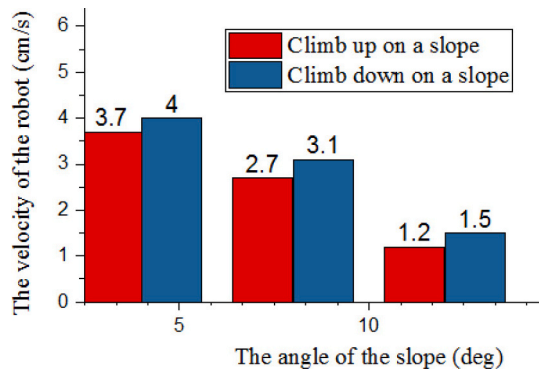


Fig. 18. Experimental results of ASRobot crawling on the slope.

As shown in Fig. 15 (a), crawling experiments with different cycles were carried out on smooth flat terrain in five trials, to lower the disturbance of incidental events. In each trial, record the time and the moving distance, the robot velocities were obtained as shown in Fig. 15 (b). The highest velocity is up to 6.05 cm/s at the cycle of 2s.

Besides the crawling gaits, we also conducted experiments of the rotary gait, i.e., rotate to the left and right with zero-radius. As shown in Fig. 16 (a), a circle board marked angle ruler was utilized to record the rotary angle the robot. Dividing the rotary time, the angular velocities of the rotation locomotion were obtained. As depicted in Fig. 16 (b), the cycle time of rotary gaits were set as 2.0s, 2.3s, 2.6s, 2.9s, 3.2s, 3.5s, 3.5s, 3.8s, 4.1s, and the highest angular velocities is up to 16.3 deg/s on the flat and smooth ground. In this experiment, below this frequency of 0.5Hz, the robot is able to rotate steadily; whereas above this frequency, an unstable phenomenon will appear.

(1) Experiments on the Slope

As for the amphibious robot, the ability of crawling on the slope in the amphibious field is important. To test the performance of climbing

on the slope, we carried out experiments on different slopes with the incline angle of 4 deg, 8deg and 12deg using the designed climbing gait on the slope. Fig. 17(a)-(d) show snapshots of ASRobot walking steadily on the slope with 10 deg. The experimental results are shown in Fig. 18. Owing to the influence of the robot gravity, the velocity of climbing down is about 0.4cm/s higher than the velocity of climbing up the slope. Without gait adjustment, the maximum incline angle of the slope the robot can climb up is only 7 deg. Using gait adjustment, the maximum angle is up to 14 deg, which is less than 18 deg. Using the precision machining technology, assembly deviations also exist in robot assembly process and will affect the performance of climbing the slopes with more than 14 deg. Another reason is the slide between the toes and the slopes. Rubber shoes make the robot climb on the flat ground flexibly, but slides also exist while the robot climbs on slopes. The robot slides more easily on the steeper slopes. For the legged robot, the capability of climbing the slope with 14 deg is quite essential to climb the gentle slopes. In the most field, the gait adjustment mechanism can satisfy the robot requirement in both stability and mobility.

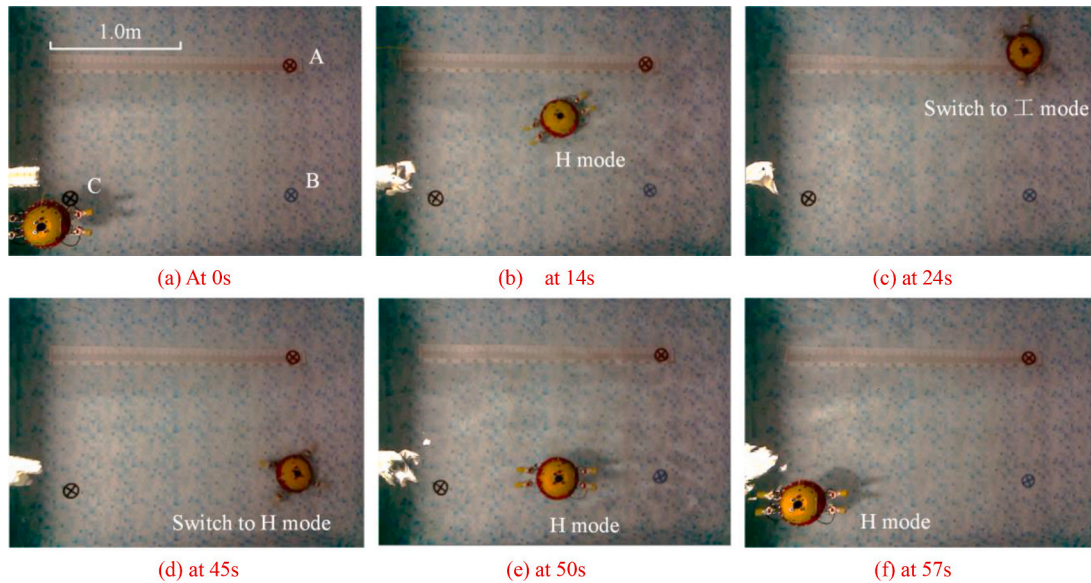


Fig. 19. Snapshots of 3-D waypoints tracking control.

5.3. 3-D Waypoints tracking with real-time dynamic thrust vectoring control

In [31], yaw control and depth control experiments were conducted and it only proves the performance of each DOF. To test 3-D underwater locomotion performance of multiple DOF, 3-D waypoints tracking experiments were carried out in the same pool. In order to realize 3-D waypoints tracking control, a vision-based positioning method is used to acquire X and Y coordinates using an external computer with a camera, and Z coordinate is obtained by pressure sensors mounted on the robot.

In this experiment, 3-D waypoints tracking is realized via the real-time dynamic thrust vectoring control. The robot started from the initial position (65cm, 170cm, -17.5cm) shown in Fig. 19(a), and then moves to three given positions A (260, 60, -50), B (260, 170, -50) and C (65, 170, -30) in turn, respectively. When the distance to the target waypoint is less than 20cm, we defined the robot arrived this waypoint. The robot began with “H” legs configuration mode with yaw angle of 0 deg. The waypoint A is in the quadrant I of the robot, and the robot did not have to switch legs configuration mode. When the robot arrived at waypoint A, waypoint B is in the quadrant IV. As shown in Fig. 19 (c), the robot switched to “I” legs configuration mode. At waypoint B, the waypoint C is in the quadrant III, the robot switched to “H” legs configuration mode as shown in Fig. 19 (d). Fig. 20(a) shows the 3-D trajectory in waypoints tracking experiment. The blue and red points indicate the start point and three preset waypoints, respectively. Fig. 20 (b) and (c) depict X (red solid curve in (b)), Y (blue solid curve in (b)) and Z (black solid curve in (c)) coordinates. The robot can rapidly move to the given waypoints. When the robot arrived at the waypoint, the robot has an inertia, which takes the robot off the waypoint. The maximum offset in X and Y coordinates is about 17cm and 5cm. The maximum depth error is about 6cm while the robot tracks waypoint A. Fig. 20 (d) shows roll, yaw and pitch angles changing in this experiment. Roll and pitch angles varied quiet slightly and the maximum offset is about 5 deg. The offset of yaw angle is a little larger from the initial position to Waypoint A, but it is still less than 40 deg. While the robot tracked waypoint B and C, the yaw angle changed less than 15 deg with switching strategy. The switching modes are shown in Fig. 20 (e). “0” and “1” indicate the “H” and “I” legs configuration modes. From these experimental results, The high precision and efficiency of 3-D waypoints tracking using “H” and “I” modes evaluated the well performance of underwater locomotion.

5.4. Various terrains test

Most amphibious robots are applied in the field area. To verify the performance of walking on various terrains, plenty of experiments have been carried out in both field and outdoor environments. As shown in Fig. 21 (a)-(f), the robot walks on asphalt ground, brisk ground, rubber ground, uneven ground, grass ground, with a water pool bottom. In the field ground, the greater friction makes the robot walk faster. The highest walking velocity and highest angular velocity are up to 6.1cm/s and 16.8deg/s on asphalt ground. Besides, walking experiment was conducted on the bottom of water. Because of the buoyancy, the friction decreases, which leads to the highest walking velocity of 4.5cm/s and the highest rotational velocity of 14.5 deg/s. Therefore, the various terrains test verified that the robot has a good performance of walking in the field environment.

5.5. Launching and landing locomotion

Compared with the robot only operating in terrestrial or aquatic environment, the crucial ability of the amphibious robot is transition locomotion from land to water and from water to land autonomously. In order to acquire robust information to realize the landing and launching locomotion, a Water Level Sensor System (WLSS) including two water-detection sensors and pressure sensors is developed to detect the environment state. From Fig. 3 (a), we can see that 12 pressure sensors are arranged around the sealed hull. The water-detection sensors are mounted on the top of the sealed hull. Only when the sealed hull sank into the water, WLSS detects the aquatic environment. When the water pressure reaches a pressure threshold, the robot will switch climbing gait to underwater locomotion and vice versa. The launching locomotion was shown in Fig. 22 (a-d). As shown Fig. 23, the blue curve indicates the average water pressure in launching locomotion. The pressure sensors start to sink into the water from a_1 point. And when it exceeds the given threshold at b_1 point, the robot switches to underwater locomotion in Fig. 22 (c). Fig. 22 (e-h) depicted the landing locomotion. Firstly, the robot swims to the bank. Owing to the inertia, the body was lifted at point b_2 . The pressure is inferior to the specific pressure, and the robot stands up and crawl to the bank from point c_2 . The robot can spend 180s in accomplishing the launching and landing locomotion. These experiments demonstrate the performance of transition from land to water and from water to land autonomously in amphibious area.

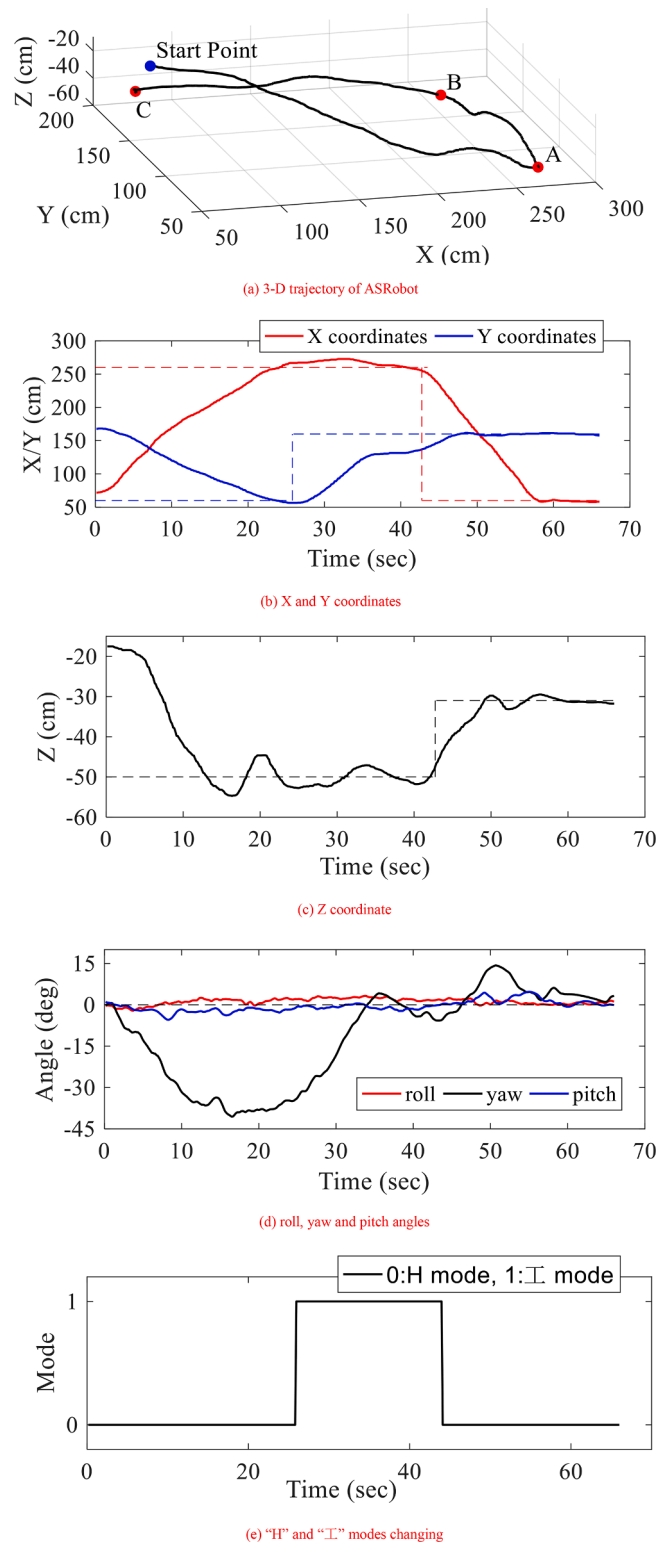


Fig. 20. 3-D waypoints tracking control.

6. Conclusions

Focusing on these applications of disaster rescue, reconnaissance and resource exploration in amphibious environments, this paper developed a detailed study on the locomotory performance of a miniature bio-inspired amphibious spherical robot with LMWCDM. This mechanism contains four legs, one of which includes three connecting rod parts, three joints actuated by servo motors and one water-jet propeller. With

gaits design using a simplified kinematic model, the robot can walk and turn flexibly on various terrains. The highest velocity and angular velocity achieved 6.1cm/s and 16.8 deg/s. Online gaits adjustment mechanism empowers the robot walk on the slope with 14 deg more stably. Real-time dynamic thrust vectoring control is proposed to enable the robot swim in water flexibly using four parallel PID algorithms and real-time dynamic vectoring allocation strategy which transform the desired force and torque calculated by PID algorithms into the water-jet

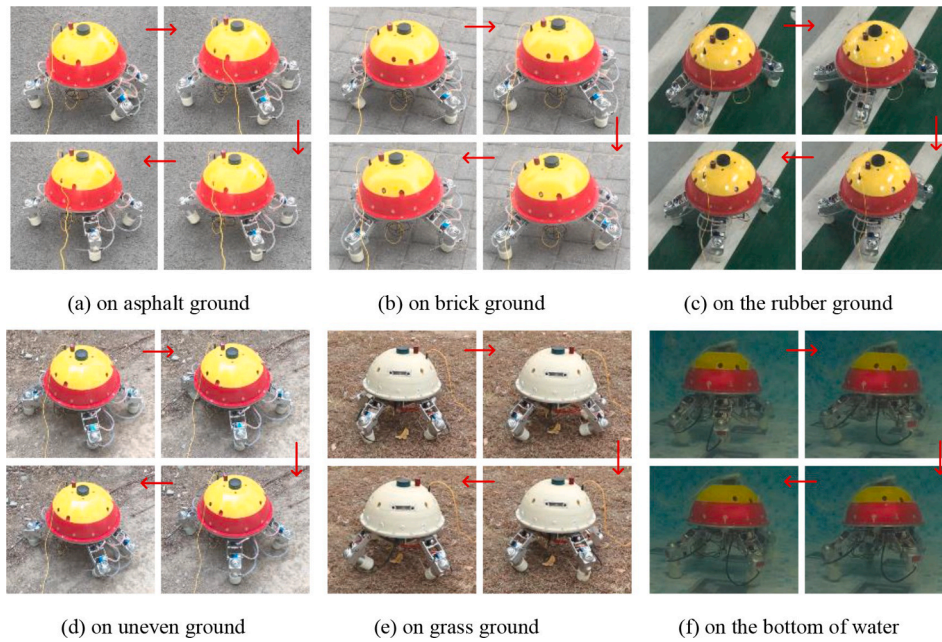


Fig. 21. Snapshots of ASRobot crawling on various terrains.

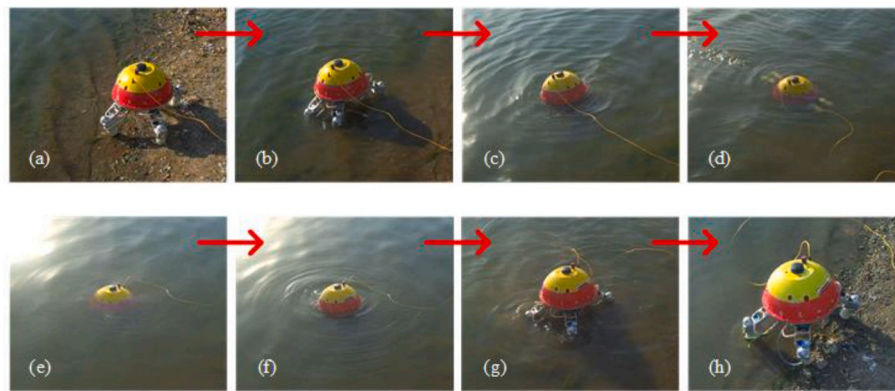


Fig. 22. Snapshots of launching motion and landing motion. (a)-(d) Launching motion; (e)-(h) landing motion.

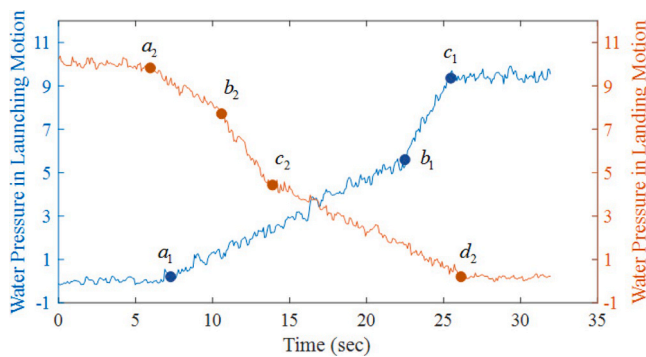


Fig. 23. Water pressure in launching and landing experiments.

and joint angles of each leg. Using real-time dynamic thrust vectoring control, 3-D waypoints tracking is realized in “H” and “工” modes, and the high precision and efficiency of 3-D waypoints tracking evaluated the well performance of underwater locomotion via “H” mode and “工” mode. Besides, the launching and landing locomotion is accomplished autonomously, which is essential to the amphibious robot.

This study will provide valuable references for the miniature amphibious robot design. Because of unaccomplished quarter-spherical hulls, the next work is fixing two hulls into the robot. And we will focus on the nonlinear controllers to improve the tracking performance.

Declaration of Competing Interest

The authors declare that they have no known competing financial interests or personal relationships that could have appeared to influence the work reported in this paper.

Acknowledgments

This work was supported by the National Natural Science Foundation of China (61773064, 61503028), National High Tech. Research and Development Program of China (No. 2015AA043202) and Graduate Technological Innovation Project of Beijing Institute of Technology (2018CX10022).

Reference

- [1] Freitas G, Lizarralde F, Liu H, Reis NRSD. Kinematic reconfigurability of mobile robots on irregular terrains. *IEEE Int Conf Robot Autom* 2009;823–8. <https://doi.org/10.117632/xwj98nb39r.1>.
- [2] Aoki T, Ito S, Sei Y. Development of quadruped walking robot with spherical shell-mechanical design for rotational locomotion. *IEEE/RSJ Int Conf Intell Robot Syst* 2015;5706–11.
- [3] Kim HG, Lee DG, Jeong KM, Seo TW. Water and ground-running robotic platform by repeated motion of six spherical footpads. *IEEE/ASME Trans Mechatron* 2016; 21(1):175–83.
- [4] Yin X, Wang C, Xie G. A salamander-like amphibious robot: system and control design. *IEEE Int Conf Mechatron Autom* 2012:956–61.
- [5] Hirose S, Yamada H. Snake-like robots: machine design of biologically inspired robots. *IEEE Robot Autom Mag* 2009;16(1):88–98.
- [6] Zhang S, Zhou Y, Xu M, Liang X, Liu J, Yang J. Amphihex-I: locomotory performance in amphibious environments with specially designed transformable flipper legs. *IEEE/ASME Trans Mechatron* 2018;23(2):1720–31.
- [7] Zhong B, Zhang S, Xu M, Zhou Y, Fang T, Li W. On a CPG-based Hexapod Robot: Amphihex-II with Variable Stiffness Legs. *IEEE/ASME Trans Mechatron* 2016;21(3):542–51.
- [8] Shen Y, Sun Y, Pu H, Ma S. Experimental Verification of the Oscillating Paddling Gait for an ePaddle-EGM Amphibious Locomotion Mechanism. *IEEE Robot Autom Lett* 2017;2(4):2322–7.
- [9] Pu H, Sun Y, Yang Y, Ma S. Modeling of the oscillating-paddling gait for an ePaddle locomotion mechanism. *IEEE Int Conf Robot Autom* 2013:3429–35.
- [10] Yang Y, Sun Y, Ma S. Paddle trajectory generation for accessing soft terrain by an ePaddle locomotion mechanism. *IEEE Int Conf Robot Autom* 2013:403–8.
- [11] Liu H, Shi L, Guo S, Xing H, Hou X, Liu Y. Platform Design for a Natatores-like Amphibious robot. *IEEE Int Conf Mechatron Autom* 2018:1627–32.
- [12] Crespi A, Ijspeert AJ. Amphibot II: an Amphibious Snake Robot that Crawls and Swims using a Central Pattern Generator. *Int Conf Clim Walk Robot* 2006: 19–27.
- [13] Guo X, Ma S, Li B, Fang Y. A novel serpentine gait generation method for snake-like robots based on geometry mechanics. *IEEE/ASME Trans Mechatron* 2018;23(3): 1249–58.
- [14] Yu S, Ma S, Li B, Wang Y. An amphibious snake-like robot with terrestrial and aquatic gaits. *IEEE Int Conf Robot Autom* 2011:2960–1.
- [15] Crespi A, Karakasiliotis K, Guignard A, Ijspeert AJ. Salamandra Robotica II: an Amphibious Robot to Study Salamander-Like Swimming and Walking Gaits. *IEEE Trans Rob* 2013;29(2):308–20.
- [16] Yu J, Ding R, Yang Q, Tan M, Wang W, Zhang J. On a Bio-inspired Amphibious Robot Capable of Multimodal Motion. *IEEE/ASME Trans Mechatron* 2012;17(5): 847–56.
- [17] Yu J, Ding R, Yang Q, Tan M, Zhang J. Amphibious Pattern Design of a Robotic Fish with Wheel-propeller-fin Mechanisms. *J Field Rob* 2013;30(5):702–16.
- [18] Ding R, Yu J, Yang Q, Tan M. CPG-based behavior design and implementation for a biomimetic amphibious robot. *IEEE Int Conf Robot Autom* 2011:209–14.
- [19] Ding R, Yu J, Yang Q, Tan M, Zhang J. Robust gait control in biomimetic amphibious robot using central pattern generator. *IEEE/RSJ Int Conf Intell Rob Syst* 2010:3067–72.
- [20] Vogel AR, Kaipa KN, Krummel GM, Bruck HA. Design of a compliance assisted quadrupedal amphibious robot. *IEEE Int Conf Robot Autom* 2014:2378–83.
- [21] Han B, Luo X, Wang X, Chen X. Mechanism design and gait experiment of an amphibian robotic turtle. *Adv Robot* 2012;25(16):2083–97.
- [22] Shi L, Guo S, Mao S, Yue C, Li M, Asaka K. Development of an amphibious turtle-inspired spherical mother robot. *J Bionic Eng* 2013;10(4):446–55.
- [23] Xing H, Guo S, Shi L, He Y, Su S, Chen Z, et al. Hybrid locomotion evaluation for a novel amphibious spherical robot. *Appl Sci* 2018;8(2):156.
- [24] Guo S, He Y, Shi L, Pan S, Xiao R, Tang K, et al. Modeling and experimental evaluation of an improved amphibious robot with compact structure. *Rob Comput Integr Manuf* 2018;51:37–52.
- [25] Xing H, Shi L, Tang K, Guo S, Hou X, Liu Y, et al. Robust RGB-D Camera and IMU Fusion-based Cooperative and Relative Close-range Localization for Multiple Turtle-inspired Amphibious Spherical Robots. *J Bionic Eng* 2019;16(3):442–54.
- [26] Han B, Luo X, Wang X, Chen X. Mechanism design and gait experiment of an amphibian robotic turtle. *Adv Robot* 2012;25(16):2083–97.
- [27] Xing H, Guo S, Shi L, Hou X, Liu Y, Liu H. Design, modeling and experimental evaluation of a legged, multi-vectored water-jet composite driving mechanism for an amphibious spherical robot. *Microsyst Technol* 2019;25(8):1–13.
- [28] Jin S, Kim J, Kim J, Seo T. Six-degree-of-freedom hovering control of an underwater robotic platform with four tilting thrusters via selective switching control. *IEEE/ASME Trans Mechatron* 2015;20(5):1–9.
- [29] Torres I, Torres J, Lozano R. A New AUV Configuration with four tilting thrusters: Navigation and Hover Tasks. *Int Conf Electr Eng, Comput Sci Autom Control (CCE)* 2021. <https://doi.org/10.1109/ICEEE.2012.6421177>.
- [30] Lopez R, Torres I, Escareno J, Salazar S, Palomino A. Quad-tilting thrusters micro submarine: modeling and Control of the attitude. *Int Conf Electron Commun Comput (CONIELECOMP)* 2021. <https://doi.org/10.1109/CONIELECOMP.2010.5440791>.
- [31] Xing H, Guo S, Shi L, Hou X, et al. A novel small-scale turtle-inspired amphibious spherical robot. 2019 *IEEE/RSJ Int Conf Intell Robots Syst (IROS)*, 3–8 Nov. 2019. <https://doi.org/10.1109/IROS40897.2019.8968304>.
- [32] Hou X, Guo S, Shi L, Xing H, Liu Y, Liu H, Hu Y, Xia D, Li Z. Hydrodynamic analysis-based modeling and experimental verification of a new water-jet thruster for an amphibious spherical robot. *Sensors* 2019;19:259.



HUIMING XING was born in Shandong, China, in 1988. He received the B.S. degree in automation from Qilu University of Technology, China, in 2013, and the M.sc in automation from Harbin Engineering University, China, in 2016. he is currently pursuing the doctor's degree in automation at Beijing Institute of Technology, China. His current research interests include amphibious robot, vision-based localization and multi-robot cooperation, etc. He has published about 24 refereed journal and conference papers in the recent years.



Liwei Shi received the B.S. degree in mechanical engineering from Harbin Engineering University, China, in 2006, the M.S. and the Ph.D. degrees in intelligent machine system from Kagawa University, Japan, in 2009 and in 2012, respectively. He was a postdoctoral researcher in Kagawa University, Japan. Currently, he is an associate professor at the Beijing Institute of Technology, he researches on underwater micro-robot utilizing artificial muscles, such as legged bio-inspired micro-robots, and spherical underwater robots, etc. He has published about 55 refereed journal and conference papers in the recent years



Xihuan Hou received the B.S. degree in automation from North China Institute of Aerospace Engineering, China, in 2014, and the M.sc in automation from Harbin Engineering University, China, in 2017. Since 2017, he has been working toward the Ph.D. degree in automation at Beijing Institute of Technology, China. His current research interests include modeling and control of an amphibious spherical robot, model predictive control, multi-robot cooperation, etc.



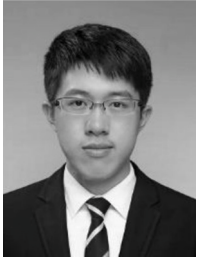
YU LIU was born in Shanxi, China, in 1997. She received the B. Sc in biomedical engineering from Beijing Institute of Technology, China, in 2017. She is currently pursuing the master's degree in biomedical engineering with Beijing Institute of Technology, China. Her current research interests include indoor localization, sensor fusion, path planning, and computer vision.



YAO HU was born in Hunan, China, in 1996. He received the B. E. degree in biomedical engineering from Beijing Institute of Technology, China, in 2018. He is currently pursuing the master's degree in biomedical engineering at Beijing Institute of Technology, China. His current research interests include amphibious robot, computer vision etc.



Zan Li was born in JiLin, China, in 1997. He received the B.S. degree in automation from TianJin University of Technology, China, in 2018. In the same year, he is pursuing the master's degree in automation at Beijing Institute of Technology, China. His current research interests include amphibious spherical robot, natatores robot, control algorithm and multi-robot cooperation, etc.



DEBIN XIA was born in Anhui, China, in 1997. He received the B.S. degree in automation from China University of Petroleum (Beijing), China, in 2018. He is currently pursuing the master's degree in biomedical engineering at Beijing Institute of Technology, China. His current research interests include amphibious robot, computer vision and multi-robot cooperation, etc.



SHUXIANG GUO was born in Jilin, China in 1963. He received the Ph.D. degree from Nagoya University in 1995. He is currently a professor in Biomedical engineering at Beijing Institute of Technology and Kagawa University, Japan. He is the leader of Key Laboratory of Convergence Biomedical Engineering System and Healthcare Technology, The Ministry of Industry and Information Technology, China. He is the Editor in Chief of IJMA (International Journal of Mechatronics and Automation). His research interests include surgical robotics, rehabilitation robotics, endoscopic capsule robotics, under water robotics.